International Journal of Botany Studies
ISSN: 2455-541X; Impact Factor: RJIF 5.12
Received: 09-04-2020; Accepted: 11-05-2020: Published: 21-05-2020
www.botanyjournals.com
Volume 5; Issue 3; 2020; Page No. 79-86

Role of *tridax procumbens* in green synthesis of cerium oxide nanoparticles and its effect on blood coagulation cascade and platelet aggregation

Vinod Gubbiveeranna[1], Pavan Kumar MA[2], Kusuma CG[3], Bhavana S[4], Sumachirayu CK[5], Sneharani AH[6], Suresh D[7] Nagaraju S[8*]

[1, 3, 4, 5, 8] Department of Studies and Research in Biochemistry, Tumkur University, Tumakuru, Karnataka, India.
[2, 6] Department of Studies in Biochemistry, Jnanakaveri PG Centre, Chikka Aluvara, Mangalore, Karnataka, India.
[7] Department of Chemistry, Tumkur University, Tumakuru, Karnataka, India

Abstract
Plant extracts play a major role in influencing the synthesis of metal oxide nanoparticles. Cerium oxide nanoparticles (CeO_2-NPs) have demonstrated promising methodologies as remedial specialists in clinical sciences. The physicochemical properties of CeO_2-NPs such as size, surface charge and agglomeration status in fluid assumes significant jobs in a definitive communication of the NPs with target cells. Recently, CeO_2-NPs have been combined through a few bio-coordinated techniques applying regular and natural lattices to prepare biocompatible CeO_2-NPs by solution combustion synthesis. A liquid concentrate of *Tridax procumbens* was used as a diminishing expert for the green association of CeO_2-NPs to form TP-CeO_2-NPs. The significance of using the plant extract in the synthesis of TP-CeO_2-NPs was characterized by Powder X-Ray Diffraction (XRD), Field Emission Scanning Electron Microscopy (FESEM), UV-Visible and Fourier-transform infrared spectroscopy (FTIR) examinations. XRD diffractograms revealed the unadulterated cubic ceria arrangement with fluorite structure having crystallite quantities to the extent of 10 – 50 nm. FESEM analysis showed the penetrable nanostructured materials. UV-Visible range demonstrated trademark osmosis generally outrageous at 342 nm. The sharp tops in the FTIR range confirmed the presence of Ce-O extending mode. The biological characterization revealed the procoagulant property of the TP-CeO_2-NPs. The higher concentration of the TP-CeO_2-NPs evaded the requirement of calcium chloride to coagulate the blood plasma as evidenced in activated partial thromboplastin time (APTT) assay. TP-CeO_2-NPs enhanced the aggregation of platelets and the NPs were devoid of hemolytic property.

Keywords: cerium oxide, *Tridax procumbens*, FESEM, XRD, FTIR, APTT, platelet aggregation

1. Introduction
In the course of the most recent decade, metal and metal-oxide nanoparticles study is a rising field in nanoscience and innovation [1]. The size and state of nanomaterials essentially assume an indispensable job in physical, electrical and optical properties [2, 5]. Cerium has been placed in the class of lanthanide series in the periodic table [6]. Cerium has a fluorite structure in an oxide state. The nanoscale structure of cerium oxide nanoparticles (CeO_2-NPs) holds the fluorite structure with oxygen inadequacies. This yields CeO_2-NPs with (CeO_2−X) opportunities which give possibilities to decrease oxidation reactions [7]. CeO_2-NPs have the potential to relieve oxidative stress, which has been connected to the improvement of neurodegenerative ailments such as Parkinson's and Alzheimer's illness. The capacity of CeO_2-NPs to switch between valency states empowers them to copy explicit compound capacities such as superoxide dismutase (SOD), catalase (CAT), phosphatase, oxidase peroxidase and phosphotriesterase [8,9]. CeO_2-NPs have likewise been accounted to have multienzyme properties, including superoxide-oxidase, catalase-oxidase and mimetic properties which aided in developing an intriguing material in natural fields such as bioanalysis [10, 15], biomedicine [16] and/or medication delivery [17,18]. These applications are gained from a speedy change of the oxidation state somewhere in the range of Ce^{3+} and Ce^{4+} [7]. The surface Ce^{3+}: Ce^{4+} proportion is affected by the microenvironment. Accordingly, the microenvironment and blend strategy received additionally assumes a significant job in deciding the natural movement and poisonous quality of CeO_2-NPs [19].

Plants have been extensively used in recent research owing to their various therapeutic potential in traditional medicinal practices. Plants are eco-friendly, inexpensive and non-toxic in nature. The presence of different constituents such as alkaloids, terpenoids, phenols, flavonoids, tannins and quinines in the plants are known to mediate in the synthesis of nanoparticles [20, 21]. These characteristics influence in incorporating plants as fuel for the green synthesis of nanoparticles [22, 23]. *Tridax procumbens* is known to possess alkaloids, steroids, carotenoids, flavonoids, phytosterols and other phytochemicals. The plant is used in Ayurvedic medicinal practice to treat diabetes, arthritis, inflammation and open wounds. Earlier research has shown that concoctions of *T. procumbens* is associated with medicinal applications such as antioxidant, anti-bacterial, anti-microbial, anti-leishmanial, anti-hepatic, vasorelaxant and mosquitocidal activities [24]. *T. procumbens* has a serine protease associated with procoagulant activity [25]. *T. procumbens* have been used as a fuel in the preparation of different nanoparticles such as silver [21, 26, 27], copper [28, 29], iron [30, 31], chromium [32] and gold [33]. This is the first report on the synthesis of chromium oxide nanoparticles with the association of *T. procumbens*.

In this study, *T. procumbens* is used as a reducing agent in the biosynthesis of cerium oxide nanoparticles. The significance of plant extract in the biosynthesis of cerium oxide nanoparticles is analyzed by comparing and characterizing the nanoparticles synthesized in the presence and absence of the plant extract, individually. The nanoparticles are also tested for its effect on blood coagulation cascade, platelet aggregation and red blood corpuscles to investigate its biological application.

2. Materials and Methods

2.1 Chemicals

Adenosine diphosphate (ADP) was purchased from Sigma Aldrich (St. Louis, MO, USA). APTT kit was purchased from Tulip Diagnostics Pvt Ltd. The remaining reagents used in these experiments were of analytical grade.

2.2 Plant material

The *T. procumbens* plant was collected near Gubbi, about 20 Km from Tumkur district, Karnataka, India (GPS 13.30°51'27" N, 76.95°25'26" E). The plant was authenticated by Dr. P. Sharanappa, Professor, Department of Studies and Research in Bioscience, Hemagangotri, University of Mysore, Hassan, India. Specific voucher specimens (TU15DOSRBC001) of this plant were deposited in the Herbarium of Department of Studies and Research in Botany, Tumkur University, Tumakuru, Karnataka, India for future reference.

2.3 Preparation of plant extract

Tridax procumbens plant was washed, shade-dried, pulverized in a blender and stored in airtight containers at 4 °C until further use. The powdered plant was extracted in distilled water in the ratio of 1:10 in a reflux arrangement at 60-70 °C for 10 hours. The extract was filtered and centrifugation was followed to remove undissolved material. The extract was then concentrated to its 1/5th of the volume in the rotatory vacuum evaporator and stored in airtight containers at 4 °C.

2.4 Preparation of CeO_2 nanoparticles (CeO_2-NPs)

Nanoparticles were prepared by the solution combustion method by using aqueous extract of *T. procumbens* as fuel [23]. A stoichiometric amount of Ceric ammonium nitrate $[(NH_4)_2Ce(NO_3)_6]$ was dissolved in 5 mL of plant extract. About 1 mL of double distilled water was added to the mixture and was kept in a preheated muffle furnace at 400 °C. After 10-15 min, golden yellow amorphous powder (TP-CeO_2-NPs) was obtained which indicated the formation of NPs. The reaction was repeated with 5, 10, 15, 20, 25 and 30 mL of the plant extract. The CeO_2-NPs was also synthesized without fuel to analyze the importance of fuel. The obtained nanoparticles were ground using mortar and pestle and stored in airtight containers until further use.

2.5 Morphological and structural characterization of nanoparticles

The crystalline structure and phase purity were examined by X-ray diffraction (XRD) (Shimadzu-7000) using Cu K_α (1.541 Å) radiation with a nickel filter operating at a voltage of 50 kV and a current of 30 mA (2θ ranging between 20° to 80°). UV–Visible spectrophotometer (Evolution-220, ThermoScientific) was used to analyze the optical properties of NPs at a resolution of 1 nm between 280 to 800 nm. The surface morphology of NPs was studied by Field Emission Scanning Electron Microscopy (FESEM) (Carl Zeiss FESEM) with 10 kV acceleration voltages. The FESEM analysis was performed by placing the samples on carbon-coated tape, air-dried and used for imaging. Detection of metals in the prepared samples was carried out using EDX attached with FESEM. Chemical constituents present in the sample were recorded by Fourier-transform infrared spectroscopy (FTIR) analysis (Model AIM-8800) under the spectral range of 4000-400 cm^{-1} with a resolution of 4 cm^{-1}. The optical properties of the NPs were characterized by Thermo Scientific Evolution-220 UV-Visible Spectrophotometer. All the experiments performed were repeated thrice for CeO_2-NPs and TP-CeO_2-NPs separately and the data were analyzed using Origin 8 software.

2.6 Effect of nanoparticles on activated partial thromboplastin time (APTT)

The CeO_2-NPs and TP-CeO_2-NPs were analyzed separately to check for its effect on blood coagulation cascade by activated partial thromboplastin time (APTT) assay as described earlier using commercial kits [25]. Human blood was treated with sodium citrate (3.2%) in the ratio of 9:1. The anticoagulated blood was centrifuged to separate platelet-poor plasma (PPP) for 5 min at 3000 rpm. About 20 mg of NPs were dispersed in 1 mL of distilled water and sonicated for 15 min at room temperature. PPP (100 µL) was incubated with different concentration of NPs for 5 min at 37 °C. After incubation, about 100 µL of commercially available APTT reagent containing activated cephaloplastin (liquicellin E) was added and incubated for 5 min at 37 °C. The clotting of the blood plasma was initiated with the addition of 25 mM $CaCl_2$ (100 µL) and the time taken to form the clot was recorded.

2.7 Effect of nanoparticles on platelet aggregation

Platelet aggregation was monitored by the colorimetric method. Platelet-rich plasma (PRP) was obtained by centrifuging the anticoagulated human blood for 15 min at 900 rpm. The supernatant obtained (PRP) was collected and transferred to a clean and dry test tube. The remaining blood was centrifuged for 20 min at 3000 rpm. The supernatant obtained was PPP, transferred to a clean and dry test tube. PPP and PRP were prewarmed to 37 °C. PRP (500 µL) was transferred to a siliconized glass cuvette and aggregated with the addition of 10 µM adenosine diphosphate (ADP) as an agonist and the aggregation was monitored every 1 min on a UV–Visible spectrophotometer at 620 nm. The effect of NPs was analyzed by incubating PRP with different concentration of CeO_2-NPs and TP-CeO_2-NPs, separately for 5 min before the addition of ADP. PPP was used as blank and the aggregation was monitored for a change in absorbance of PPP and PRP with the agonist representing 0% and 100%, respectively.

2.8 Hemolytic assay

The hemolytic assay was performed to analyze the effect of NPs on mammalian erythrocytes.

Preparation of erythrocyte suspension: Anticoagulated human blood was centrifuged for 5 min at 3000 rpm. The pellet consisting of the red blood corpuscles (RBC) cells were carefully separated and washed with saline (0.9%) for three times. Two percent of erythrocyte suspension was made by suspending RBC cells in saline.

Hemolytic activity: In vitro hemolytic activity was performed according to the method described earlier [34]. Different concentration of CeO_2-NPs and TP-CeO_2-NPs were added separately to test tubes containing 0.5 ml of the erythrocyte suspension prepared earlier and made up to 1 mL with saline. The test tubes were incubated for 30 min at 37 °C. After incubation, the mixture was made up to 2 mL with saline and centrifuged to separate the RBC for 3 min at 1500 rpm. One mL of the supernatant was transferred to a siliconized glass cuvette and analyzed for the amount of free hemoglobin at 540 nm. Saline and sodium dodecyl sulfate (SDS) detergent were used as minimal and maximal hemolytic controls.

2.9 Statistical analysis
All the results of the experiments were performed in triplicates and expressed as mean ± standard error of the mean (SEM). The results were statistically analyzed using one–way ANOVA followed by Tukey's Multiple Comparison Test. The data were considered significant at $p < 0.05$.

3. Results and Discussion
3.1 XRD of TP-CeO_2-NPs
The phase compositions of the CeO_2-NPs and TP-CeO_2-NPs were analyzed by X-ray diffraction. The XRD patterns of the NPs were compared with standards compiled by the Joint Committee on Powder Diffraction and Standards (JCPDS). The crystallite sizes of the NPs were calculated using Debye Scherrer formula:

$$D = \frac{0.89\lambda}{\beta Cos\theta}$$

To calculate the lattice strain of the NPs specimens, the Williamson-Hall method was applied [35]:

$$\beta\cos\theta = \frac{0.9\lambda}{D} + 4\eta\sin\theta$$

Where, λ, D, η and θ are the wavelength of the X-ray used (0.154056 nm), crystallite size, internal micro-strain associated with it and the Bragg angle (θ), correspondingly. Note that β in the above equation is the peak width (in radians) after subtracting the peak width due to instrumental broadening from the experimentally recorded pattern. Therefore, when βcosθ was plotted against 4sinθ, straight lines were obtained with the slope as η and the intercept as 0.9λ/D. The XRD pattern of the CeO_2-NPs and TP-CeO_2-NPs are shown in Fig. 1 and 2, respectively. The XRD peak positions were reliable with the cerium oxide. These are in good agreement with those in the JCPDS card (Card No. 89-1397). The presence of (110), (111) and (202) planes in XRD indicates the formation of the pure monoclinic structure of TP-CeO_2-NPs. No peaks were detected due to impurities, infers the high purity of TP-CeO_2-NPs synthesized by this method.

The sharp and narrow diffraction peaks of CeO_2 indicate that the resulting products were of high crystalline in nature. By using the Scherrer formula, the crystallite size for any three different concentrations of CeO_2-NPs synthesized was found to be between 8 and 13 nm. The average crystallite size was found to be in the range of 12 to 20 nm for any three different concentrations of TP-CeO_2-NPs. This observation of the formation of narrow and uniform particles unambiguously demonstrates the role of fuel.

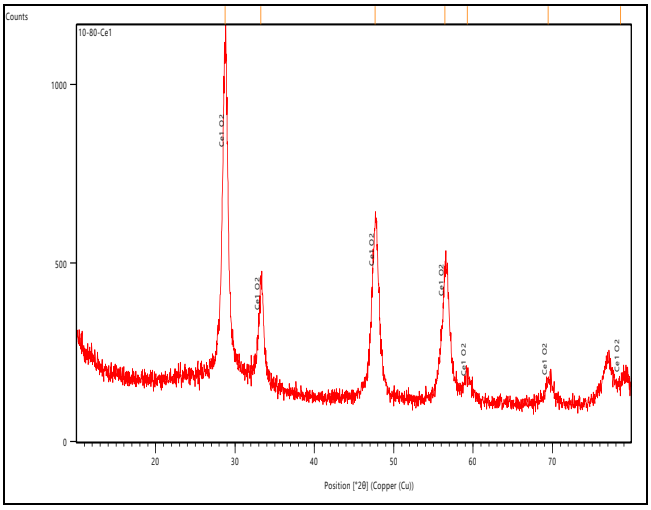

Fig 1: X-ray diffraction patterns of CeO_2-NPs

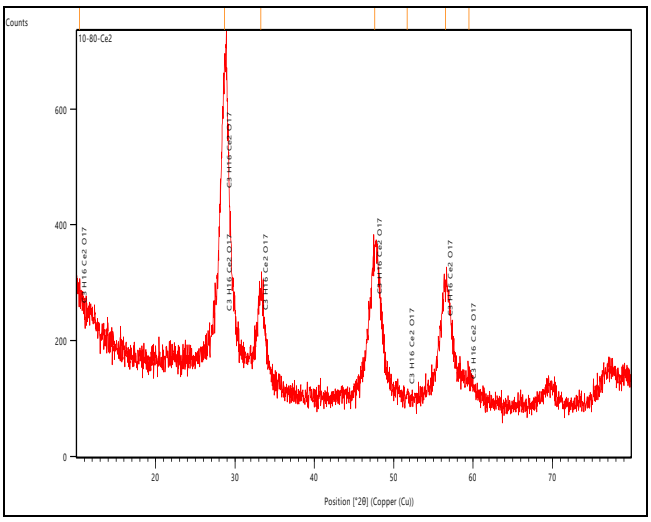

Fig 2: X-ray diffraction patterns of TP-CeO_2-NPs

3.2 UV-Visible spectrum of TP-CeO_2-NPs
The synthesized CeO_2-NPs and TP-CeO_2-NPs were examined by UV-Visible spectrophotometer and results are plotted in the graph (Fig. 3 and 4, respectively). The UV–Visible spectrum exhibited a well-defined absorption band at 365 nm and 342 nm confirming the formation of CeO_2-NPs and TP-CeO_2-NPs, respectively.

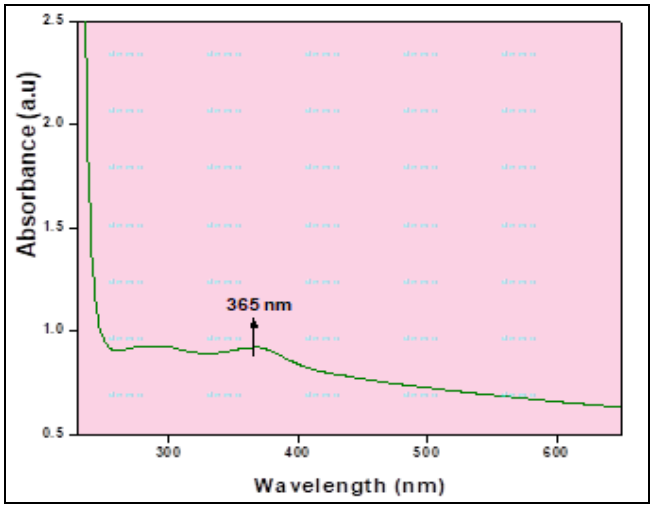

Fig 3: UV-Visible spectrum of CeO_2-NPs

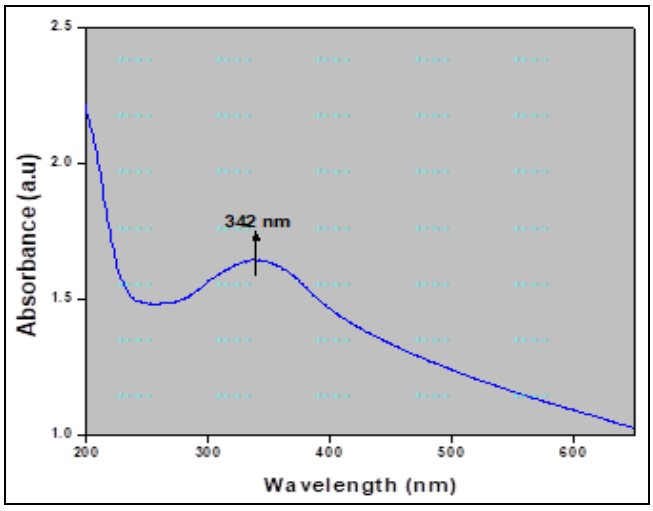

Fig 4: UV-Visible spectrum of TP-CeO_2-NPs

3.3 FESEM-EDX of TP-CeO_2-NPs

FESEM pictures exhibit the development of whip-like permeable NPs during the arrangement ignition union of TP-CeO_2-NPs. During arrangement burning, enormous volumes of gases were developed as a result of the debasement of metal nitrates. Little particles were framed because of the break of the gases under high tension. The FESEM pictures uncovered that the CeO_2-NPs (Fig. 5) and TP-CeO_2-NPs (Fig. 6) arranged with enormous size having a circle-like structure with normal molecule size. A quantitative component mapping of CeO_2-NPs (Fig. 7) and TP-CeO_2-NPs (Fig. 8) was completed utilizing the EDX investigation to describe the segments joined to the flank surface. The mapping brings about that CeO_2-NPs show just cerium components (Table 1) and TP-CeO_2-NPs show different components alongside cerium (Table 2).

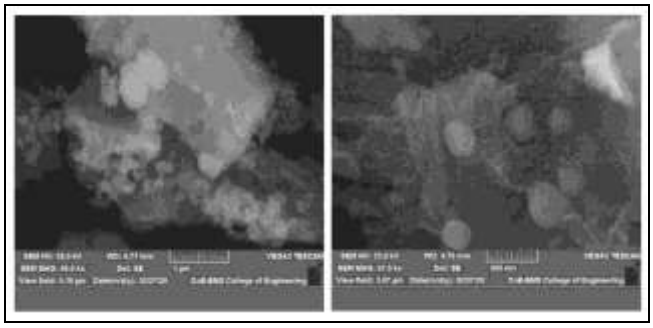

Fig 5: FESEM images of CeO_2-NPs

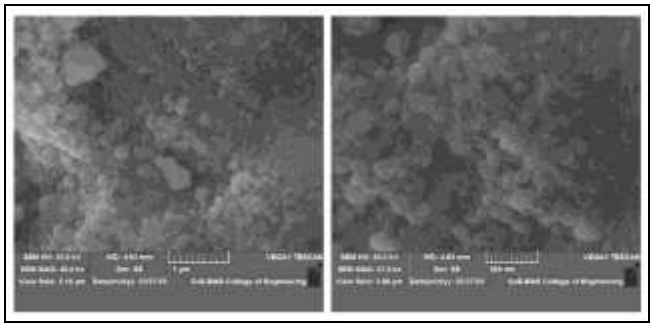

Fig 6: FESEM images of TP-CeO_2-NPs

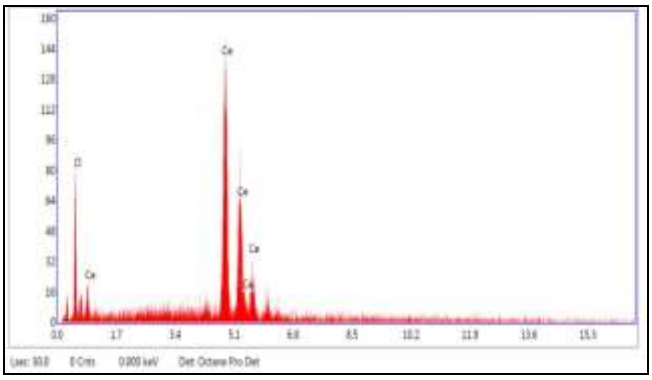

Fig 7: EDX of CeO_2-NPs

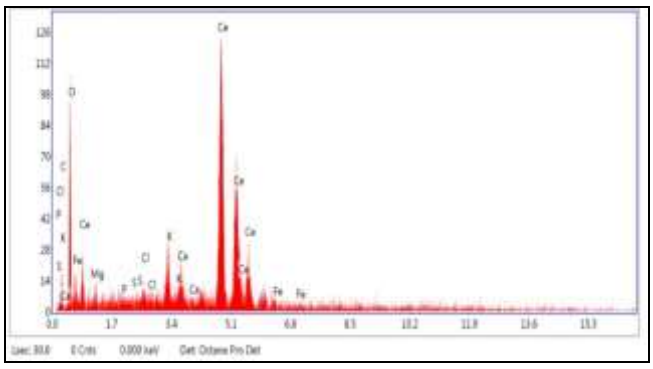

Fig 8: EDX of TP-CeO_2-NPs

Table 1: Elemental analysis of CeO_2-NPs by XRD

S. No.	Element	Weight %	Atomic %
1	O K	18.80	66.97
2	CeL	81.20	33.03

Table 2: Elemental analysis of TP-CeO_2-NPs by XRD

S. No.	Element	Weight %	Atomic %
1	C K	5.66	17.03
2	O K	25.33	57.23
3	MgK	1.98	2.95
4	P K	0.82	0.95
5	S K	0.19	0.21
6	ClK	0.67	0.68
7	K K	3.04	2.81
8	CaK	2.55	2.30
9	CeL	58.71	15.15
10	FeK	1.06	0.68

3.4 FTIR of TP-CeO_2-NPs

The FTIR of CeO_2-NPs and TP-CeO_2-NPs were in the scope of 400-4000 cm^{-1} wave number which recognizes the synthetic bonds just as practical gatherings in the compound. In Fig. 9, the enormous expansive band at 3418.98 cm^{-1} is attributed to the O-H extending vibration in OH− gatherings. The retention is top around 2925 cm^{-1}, is allocated to the bowing vibration of C-H extending. The extreme band at 557.94 cm^{-1} relates to the Ce-O extending vibration [36,37]. The band situated at 1060.36 and 1331.31 cm^{-1} has been ascribed to the CO_2 topsy-turvy extending vibration and C-O extending vibration, individually. In the fig. 10, the band at 3420.18 cm^{-1} is attributed to the O-H extending vibration in OH− gatherings. The sharp and exceptional top around 1384.51 cm^{-1} is attributed to the bowing vibration of C-O extending. The band at 513.05 cm^{-1} compares to the Ce-O extending vibration.

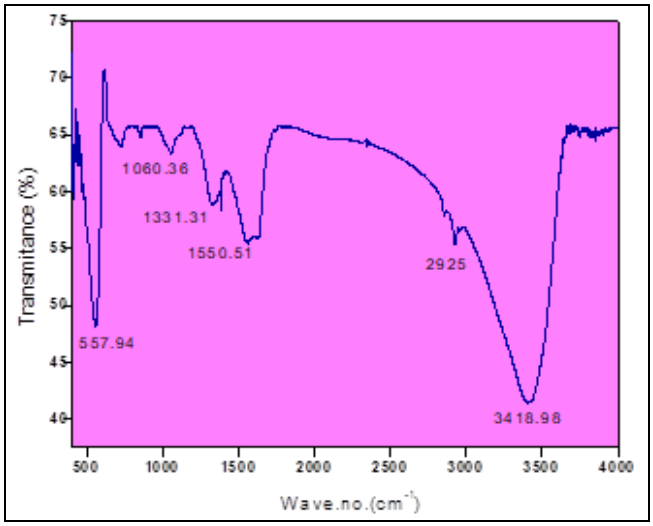

Fig 9: FTIR spectrum of CeO_2-NPs

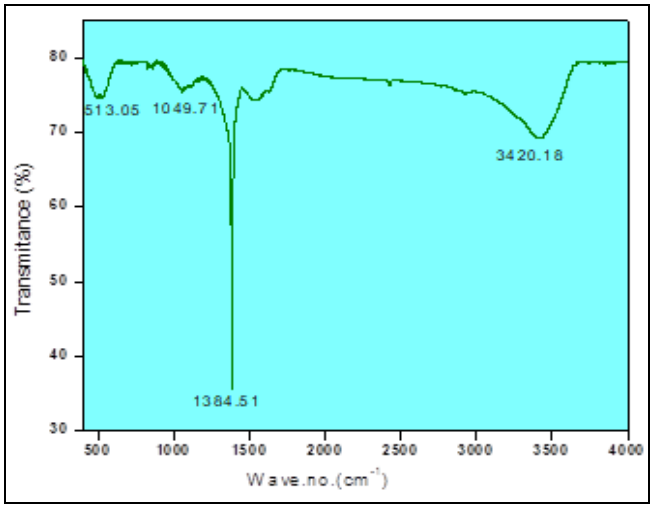

Fig 10: FTIR spectrum of TP-CeO_2-NPs

3.5 Activated partial thromboplastin time

TP-CeO_2-NPs interfered with the contact activation pathway of the blood coagulation cascade, as evidenced by the APTT assay. The APTT reagent, Liquicellin E is a phospholipid containing activated cephaloplastin reagent. Cephaloplastin activates the coagulation factors involved in the contact activation pathway such as factor VIII, IX, XI and XII. The activated factor IX (FIXa) in the presence of activated factor VIII (FVIIIa), phospholipid and calcium ions activate factor X (FX) to factor Xa (FXa). The FXa with FVa, phospholipid and calcium ions as the cofactors, converts prothrombin to thrombin. The thrombin immediately converts fibrinogen to fibrin and activates FXIII to FXIIIa. The activated FXIIIa stabilizes the soluble fibrin clot and promotes the formation of an insoluble hard clot. CeO_2-NPs showed a very mild anticoagulant effect on the APTT. The normal APTT was found to be 38.24 s and with 1000 µg of CeO_2-NPs the clotting time was increased to 64.74 s. The fuel affected the anticoagulant nature of CeO_2-NPs when it was synthesized in the presence of the *T. procumbens* (TP-CeO_2-NPs) into procoagulant nature in a dose-dependent manner (Fig. 11, $^{**}p < 0.01$, *and* $^{***}p < 0.001$). TP-CeO_2-NPs (800 µg) decreased the coagulation time of APTT from 38.24 s to 6.81 s (Table 3). Interestingly, the higher concentration of TP-CeO_2-NPs (>1000 µg with activated cephaloplastin reagent) coagulated the plasma evading the requirement of calcium chloride in APTT assay. Further increase in the concentration of TP-CeO_2-NPs had no significant effect in increasing the APTT (Table 4). NPs have a tendency to adsorb with the protein to form 'protein corona' and modify their biocompatibility [38,39]. Though the exact mechanism is unknown, owing to its non-protein composition, the activation of the fibrinogen enzymatically can be ruled out and the NPs might be mimicking to activate at the activation sites of the platelets and coagulation factors [40,41].

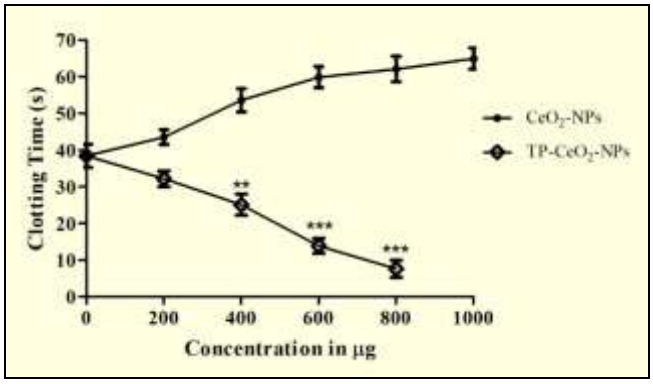

Fig 11: APTT of TP-CeO_2-NPs

Table 3: Activated partial thromboplastin time of TP-CeO_2-NPs in low concentration

	Concentration in µg	APTT reagents	APTT ins ± SEM
Control	0	Activated cephaloplastin reagent + $CaCl_2$	38.41 ± 3.18
CeO_2-NPs	200		43.50 ± 2.02
	400		53.56 ± 3.18
	600		59.83 ± 2.90
	800		62.06 ± 3.47
	1000		64.91 ± 2.89
TP-CeO_2-NPs	200		32.15 ±2.12
	400		25.06 ± 2.89
	600		13.86 ± 2.05
	800		7.60 ± 2.34

Table 4: Activated partial thromboplastin time of TP-CeO_2-NPs in high concentration

	Concentration in µg	APTT reagents	APTT ins ± SEM
TP-CeO_2-NPs	1000	Activated cephaloplastin reagent	253.46 ± 3.89
	1200		234.06 ± 7.01
	1400		222.12 ± 4.92
	1600		208.18 ± 5.33
	1800		203.56 ± 4.88
	2000		199.89 ±5.77

3.6 Platelet aggregation studies

Platelet aggregation is the first step in the blood coagulation upon injury. Platelet aggregation involves platelet-platelet adhesion and adhesion to the injured site. Platelets are activated by agonists such as ADP, epinephrine and collagen. The activation of the platelets through the receptor-agonist interaction stimulates the release of calcium ions in the cytoplasm [42]. An increased concentration of intracytoplasmic calcium ions induces a conformational change in the shape of platelets from disc to a spiny sphere with granulations all over [43]. The shape change in the platelet is allied with the cytoskeleton, microtubules and actin filaments of the platelets. This causes the projections on the morphologically modified platelets to interact with each other to form aggregates [44]. The effect of TP-CeO_2-NPs was studied spectrophotometrically using PRP. CeO_2-NPs did not affect the platelet's aggregation. However, TP-CeO_2-NPs enhanced the platelet aggregation induced by ADP. The aggregation induced by ADP alone was considered as 100% and with 2 mg of TP-CeO_2-NPs, the aggregation was enhanced to 191% at 6 min (Fig. 12, $**p < 0.01$, *and* $***p < 0.001$). The enhanced activity might be due to the interaction of TP-CeO_2-NPs with surface receptors of platelets and/or adhesion membrane protein GPIIb/IIIa [45,46].

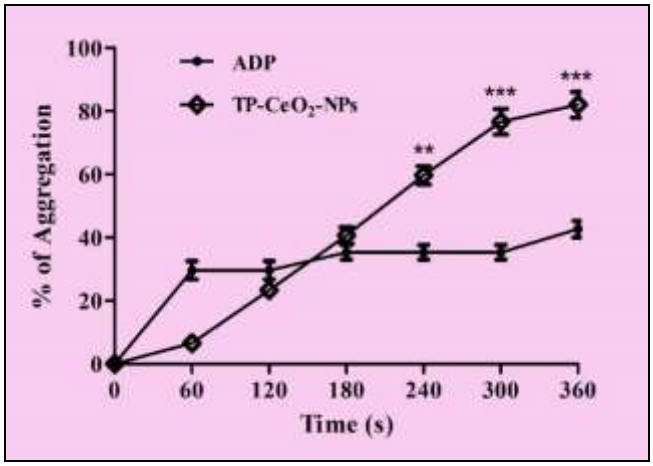

Fig 12: Platelet aggregation studies of TP-CeO_2-NPs

3.7 Hemolytic activity

Hemoglobin was not liberated with the incubation of up to 2000 µg of TP-CeO_2-NPs (data not shown). This shows that TP-CeO_2-NPs is devoid of the hemolytic property up to the tested concentration. In contrast, the positive control, SDS detergent induced hemolysis releasing free hemoglobin.

4. Conclusion

The examination shows a green strategy for the union of cerium oxide nanoparticles employing arrangement ignition strategy utilizing *T. procumbens* as fuel. The combination strategy is prudent, brisk, maintains a strategic distance from numerous response steps and destructive synthetic concoctions. TP-CeO_2-NPs is active biologically by interfering in the blood coagulation cascade and platelet aggregation. TP-CeO_2-NPs enhanced the plasma coagulation and platelet aggregation without showing the hemolytic property. This readiness/active principle of TP-CeO_2-NPs amalgamation is ecofriendly and can be adequately adjusted for a huge scope combination.

Graphical abstract

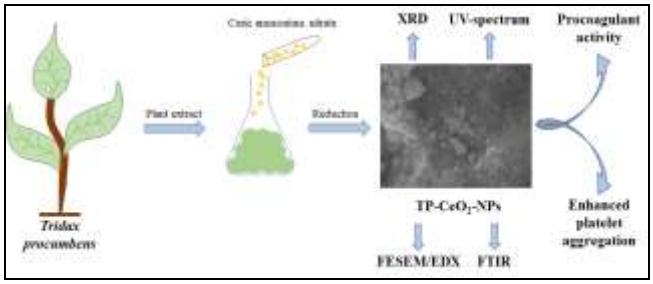

5. References

1. Chandra RGS, Ramesh TN, Gubbiveeranna V, Maiya PS. Antimicrobial activity studies of zinc oxide, zinc acetate and layered zinc hydroxysalt. Inernational J. Sci. Res. 2013; 01(04):524-530.
2. Gagnon J, Fromm KM. Toxicity and protective effects of cerium oxide nanoparticles (nanoceria) depending on their preparation method, particle size, cell type, and exposure route. Eur. J Inorg. Chem. 2015; 2015(27):4510-4517.

3. Tian Z, Li J, Zhang Z, Gao W, Zhou X, Qu Y. Highly sensitive and robust peroxidase-like activity of porous nanorods of ceria and their application for breast cancer detection. Biomaterials. 2015; 59:116-124.
4. Arya A, Gangwar A, Singh SK, Roy M, Das M, Sethy NK, *et al*. Cerium oxide nanoparticles promote neurogenesis and abrogate hypoxia-induced memory impairment through AMPK-PKC-CBP signaling cascade. Int. J Nanomedicine. 2016; 11:1159-1173.
5. Beaudoux X, Virot M, Chave T, Durand G, Leturcq G, Nikitenko SI. Vitamin C boosts ceria-based catalyst recycling. Green Chem. 2016; 18(12):3656-3668.
6. Weeks ME. The discovery of the elements. XVI. The rare earth elements. J Chem. Educ. 1932; 9(10):1751-1773.
7. Yao SY, Xu WQ, Johnston-Peck AC, Zhao FZ, Liu ZY, Luo S, *et al*. Morphological effects of the nanostructured ceria support on the activity and stability of CuO/CeO_2 catalysts for the water-gas shift reaction. Phys. Chem. Chem. Phys. 2014; 16(32):17183-17195.
8. Yang Y, Mao Z, Huang W, Liu L, Li J, Li J, *et al*. Redox enzyme-mimicking activities of CeO_2 nanostructures: Intrinsic influence of exposed facets. Sci. Rep, 2016; 6:35344.
9. Baldim V, Bedioui F, Mignet N, Margaill I, Berret JF. The enzyme-like catalytic activity of cerium oxide nanoparticles and its dependency on Ce^{3+} surface area concentration. Nanoscale. 2018; 10(15):6971-6980.
10. Asati A, Santra S, Kaittanis C, Nath S, Perez JM. Oxidase-like activity of polymer-coated cerium oxide nanoparticles. Angew. Chemie - Int. Ed. 2009; 48(13):2308-2312.
11. Asati A, Kaittanis C, Santra S, Perez JM. pH-tunable oxidase-like activity of cerium oxide nanoparticles achieving sensitive fluorigenic detection of cancer biomarkers at neutral pH. Anal. Chem. 2011; 83(7):2547-2553.
12. Li X, Sun L, Ge A, Guo Y. Enhanced chemiluminescence detection of thrombin based on cerium oxide nanoparticles. Chem. Commun. 2011; 47(3):947-949.
13. Kaittanis C, Santra S, Asati A, Perez JM. A cerium oxide nanoparticle-based device for the detection of chronic inflammation via optical and magnetic resonance imaging. Nanoscale. 2012; 4(6):2117-2123.
14. Ornatska M, Sharpe E, Andreescu D, Andreescu S. Paper bioassay based on ceria nanoparticles as colorimetric probes. Anal. Chem. 2011; 83(11):4273-4280.
15. Lin Y, Xu C, Ren J, Qu X. Using thermally regenerable cerium oxide nanoparticles in biocomputing to perform label-free, resettable, and colorimetric logic operations. Angew. Chemie - Int. Ed. 2012; 51(50):12579-12583.
16. Celardo I, Pedersen JZ, Traversa E, Ghibelli L. Pharmacological potential of cerium oxide nanoparticles. Nanoscale. 2011; 3(4):1411-1420.
17. Li M, Shi P, Xu C, Ren J, Qu X. Cerium oxide caged metal chelator: anti-aggregation and anti-oxidation integrated H_2O_2-responsive controlled drug release for potential Alzheimer's disease treatment. Chem. Sci. 2013; 4(6):2536-2542.
18. Xu C, Lin Y, Wang J, Wu L, Wei W, Ren J, *et al*. Nanoceria-triggered synergetic drug release based on CeO_2-capped mesoporous silica host-guest interactions and switchable enzymatic activity and cellular effects of CeO_2. Adv. Healthc. Mater. 2013; 2(12):1591-1599.
19. Chen HI, Chang HY. Synthesis of nanocrystalline cerium oxide particles by the precipitation method. Ceram. Int. 2005; 31(6):795-802.
20. Mukherjee P, Ahmad A, Mandal D, Senapati S, Sainkar SR, Khan MI, *et al*. Fungus-mediated synthesis of silver nanoparticles and their immobilization in the mycelial matrix: a novel biological approach to nanoparticle synthesis. Nano Lett. 2001; 1(10):515-519.
21. Vastrad J V, Goudar G. Green synthesis and characterization of silver nanoparticles using leaf extract of *Tridax procumbens*. Orient. J Chem. 2016; 32(3):1525-1530.
22. Bhavana S, Gubbiveeranna V, Kusuma CG, Ravikumar H, Sumachirayu CK, Nagabhushana H, *et al*. Facile green synthesis of SnO_2 NPs using *Vitex altissima* (L.) leaves extracts: characterization and evaluation of antibacterial and anticancer properties. J Clust. Sci. 2019; 30:431-437.
23. Suresh D, Nethravathi PC, Udayabhanu, Rajanaika H, Nagabhushana H, Sharma SC. Green synthesis of multifunctional zinc oxide (ZnO) nanoparticles using *Cassia fistula* plant extract and their photodegradative, antioxidant and antibacterial activities. Mater. Sci. Semicond. Process. 2015; 31:446-454.
24. Gubbiveeranna V, Nagaraju S. Ethnomedicinal, phytochemical constituents and pharmacological activities of *Tridax procumbens*: a review. Int. J Pharm. Pharm. Sci. 2016; 8(2):1-7.
25. Gubbiveeranna V, Kusuma CG, Bhavana S, Sumachirayu CK, Ravikumar H, Nagaraju S. Potent procoagulant and platelet aggregation inducing serine protease from *Tridax procumbens* extract. Pharmacognosy Res. 2019; 11(4):363-370.
26. Kushwaha HB, Malik CP. Biosynthesis of silver nanoparticles using fresh extracts of *Tridax procumbens* Linn. Indian J Exp. Biol. 2014; 52:359-368.
27. Tejal M, Jigna S, Prakash SSO, Ronak V, Smit P. Green synthesis of silver nanoparticles, characterization and study its wound healing property. Pharm. Anal. Acta. 2015; 6(1):141.
28. Kalpana VN, Chakraborthy P, Palanichamy V, Rajeswari VD. Synthesis and characterization of copper nanoparticles using *Tridax procumbens* and its application in degradation of bismarck brown. Int. J ChemTech Res. 2016; 9(9):498-507.
29. Selvan SM, Anand KV, Govindaraju K, Tamilselvan S, Kumar VG, Subramanian KS, *et al*. Green synthesis of copper oxide nanoparticles and mosquito larvicidal activity against dengue, zika and chikungunya causing vector *Aedes aegypti*. IET Nanobiotechnology. 2018; 12(8):1042-1046.
30. Senthil M, Ramesh C. Biogenic synthesis of Fe_3O_4 nanoparticles using *Tridax procumbens* leaf extract and its antibacterial activity on *Pseudomonas aeruginosa*. Dig. J. Nanomater. Biostructures. 2012; 7(3):1655-1660.
31. Kuchekar SR, Patil MP, Gaikwad VB, Han S. *Tridax procumben* leaf extract mediated green synthesis of iron oxide nanoparticles: spectroscopic and microscopic studies. Int. J Chem. Phys. Sci. 2018; 7:199-204.

32. Ramesh C, Kumar KM, Latha N, Ragunathan V. Green synthesis of Cr_2O_3 nanoparticles using *Tridax procumbens* leaf extract and its antibacterial activity on *Escherichia coli*. Curr. Nanosci. 2012; 8(42):603-607.
33. Rao KMS, Sekhar EC, Rao KSVK. Biosynthesis of microbial resistance Au-nanoparticles from aqueous extract of *Tridax procumbens* leaves. Indian J Adv. Chem. Sci. 2017; 5(1):24-29.
34. Gubbiveeranna V, Kusuma CG, Bhavana S, Sumachirayu CK, Nagaraju S. Anti-hemostatic protease from *Jatropha curcas* latex with fibrinogen lytic activity. J Pharmacogn. Phytochem. 2019; 8(1):1303-1310.
35. Xu C, Qu X. Cerium oxide nanoparticle: a remarkably versatile rare earth nanomaterial for biological applications. NPG Asia Mater. 2014; 6(3):e90.
36. Zhang Z, Kleinstreuer C, Donohue JF, Kim CS. Comparison of micro- and nano-size particle depositions in a human upper airway model. J Aerosol Sci. 2005; 36:211-233.
37. Mcdevitt NT, Baun WL. Infrared absorption study of metal oxides in the low frequency region (700-240 cm-1). Spectrochim. Acta. 1964; 20:799-808.
38. Treuel L, Nienhaus GU. Toward a molecular understanding of nanoparticle – protein interactions. Biophys. Rev. 2012; 4(2):137-147.
39. Gebauer JS, Malissek M, Simon S, Knauer SK, Maskos M, Stauber RH, *et al*. Impact of the nanoparticle − protein corona on colloidal stability and protein structure. Langmuir. 2012; 28(25):9673-9679.
40. Roy SC, Paulose M, Grimes CA. The effect of TiO_2 nanotubes in the enhancement of blood clotting for the control of hemorrhage. Biomaterials. 2007; 28:4667-4672.
41. Anselmo AC, Modery-pawlowski CL, Menegatti S, Kumar S, Vogus R, Tian LL, *et al*. Platelet-like nanoparticles (PLNs): engineering shape, flexibility and surface chemistry of nanocarriers to target vascular injuries. ACS Nano. 2014; 8(11):11243-11253.
42. Szabo VD, Braun A, Nieswandt B. Calcium signaling in platelets. J. Thromb. Haemost. 2009; 7:1057-1066.
43. Gryglewski RJ. Prostacyclin among prostanoids. Pharmacol. Reports. 2008; 60:3-11.
44. Fox JEB. Cytoskeletal proteins and platelet signaling. Thromb. Haemost. 2001; 86:198-213.
45. Hante NK, Medina C, Santos-martinez MJ. Effect on platelet function of metal-based nanoparticles developed for medical applications. Front. Cardiovasc. Med, 2019; 6:139.
46. Niiya K, Hodson E, Bader R, Byers-Ward V, Koziol JA, Plow EF, *et al*. Increased surface expression of the membrane glycoprotein IIb/IIIa complex induced by platelet activation. Relationship to the binding of fibrinogen and platelet aggregation. Blood. 1987; 2:475-483.